Analysis of Huffman's Hexagonal Column with Cusps

Klara Mundilova, Erik D. Demaine, Robert J. Lang, Tomohiro Tachi

Abstract:

We analyze the mathematical existence of one of David Huffman's most prominent curved-crease designs: the Hexagonal Column with Cusps, featuring circular, parabolic, and straight creases. Observations of the physical folded shape suggest that the concave regions between two parabolas form a cylinder, and the regions between the circle and the nearest intersection of the parabolas form a cone. In our analysis, we deduce the remaining rulings that result in a numerically closed hexagonal shape. Finally, we explore other variations of the shape, including those that incorporate only circular creases.

1 Introduction

Folding paper along curved creases produces a variety of intricate shapes that find application in artistic exploration dating back to the Bauhaus in 1927, along with foundational contributions by Huffman and Resch in the late 1900s [Demaine et al. 15a]. Contemporary origami artists who use curved creases include Erik and Martin Demaine, Robert Lang, Ekaterina Lukasheva, Jun Mitani, Jeanine Mosely, Saadya Sternberg, and Polly Verity.

Curved creases are also practical for cost-efficient fabrication as they offer a rich family of complex 3D shapes from relatively few creases. Folding paper by hand along curved creases is an accessible way to explore the variety of possible shapes. But practical applications require a precise digital model for analyzing features such as structural stiffness. Unfortunately, the task of digitally designing accurate and smooth folded shapes presents significant challenges. An important step toward developing suitable design tools is gaining a better understanding of the geometry of existing folded designs and their folding behavior.

In the quest for a precise mathematical description, a first abstraction step is to replace flat sheets of material with mathematical surfaces that can be flattened (developed) into the plane without stretching or tearing, known as *developable surfaces*. Such surfaces are well-studied in classical differential geometry and are characterized by a family of straight lines, known as *rulings*, each met by a single tangent plane to the surface. When mathematically reconstructing a curved-crease folded design, we segment the shape into individual smooth developable surfaces, which we call *developable patches*. When the design comes from a flat sheet of

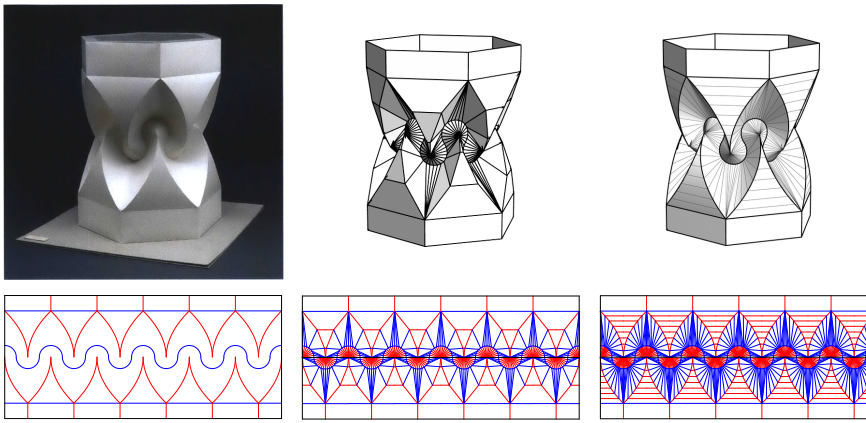

Figure 1: *Hexagonal Column with Cusps (David Huffman, 1978) and corresponding crease patterns. Left: Original folding (Figure 4.4.48 in [Koschitz 14]). Used with permission of the Huffman family. Center: Discretization by [Demaine et al. 18]. Right: Smooth reconstruction presented in this paper.*

paper, the curved boundaries of two adjacent developable patches are identical in their development.

A crucial part of the analysis of a folded shape is to identify and parameterize the rulings of the developable patches. In the few instances where an accurate prediction of these rulings is possible, analyzing the corresponding shape tends to be straightforward. Notable examples include Mosely's analysis of her design, the "Orb" [Mosely 02], and the parameterization of the folded Vesica Piscis by [Mundilova and Wills 18]. Demaine et al. demonstrate the existence of lens tessellations with convex curves [Demaine et al. 15b], and analyze many of David Huffman's designs that use conics as creases [Demaine et al. 18].

However, in the vast majority of artistic curved crease designs, guessing or analyzing the rulings is not straightforward. This becomes particularly problematic when more than one crease is involved, as not all ruling assignments are feasible. The rulings must satisfy certain geometric constraints, and this can lead to an overconstrained system. Generally, an optimization-based approach is necessary to determine the rulings of a shape [Kergosien et al. 94].

In the analysis that follows, we examine David Huffman's Hexagonal Column with Cusps; see Figure 1. [Demaine et al. 18] demonstrate that the choice of "natural" rulings does not lead to a folded state, though parts of the rulings can be deduced from assumptions about the shape. The authors introduce a discrete approximation that suggests an alternative ruling, and we show here a smooth analogue that bears similarity.

The main difficulty in the analysis of the Hexagonal Column is the assignment of rulings to three consecutive patches. Observing the physical folded shape, we can make educated guesses about the rulings of the first and last patch: the concave

regions between two parabolas appear to form a cylinder (parallel rulings), and the regions between the circle and the nearest intersection of the parabolas appear form a cone (converging rulings). In this paper, we provide a computational framework to find the rulings of the central patch when given the rulings of its two neighboring patches. By contrast, previous work by [Alese 22] explores the propagation of rulings across creases, a method which is suitable if you can establish the rulings for two adjacent patches, which does not apply here.

Our paper is structured as follows: First, we review some known theory on developable surfaces and the parametrizations of a single curved crease. In Section 3, we consider a combination of three patches joined along two creases and demonstrate how to determine the rulings of a central patch when the rulings of its adjacent patches are specified. We apply these findings to the Hexagonal Column in Section 4. Finally, in Section 4.5, we explore some variations of the crease pattern.

2 Curved Folding Primer

In this section, we establish the foundation of our analysis of shapes from developable surfaces. We follow the notation used by [Mundilova 23], which builds upon works of [Demaine et al. 15b, Demaine et al. 18].

2.1 Parametrization of Developable Surfaces

In the following, we parametrize developable surfaces as ruled surfaces while imposing an additional constraint to ensure developability.

2.1.1 Ruled Surfaces

We parametrize a *ruled surface* as

$$\mathbf{S}(t,u) = \mathbf{X}(t) + u\mathbf{R}(t), \tag{1}$$

where $\mathbf{X}(t) : T \to \mathbb{R}^3$ is a curve, the *directrix*, and $\mathbf{R}(t) : T \to S^2$ are unit-length vectors, the so-called *ruling directions*. Without loss of generality, we assume $T = [0, t_{\max}]$, for some $t_{\max} > 0$, and $u \in \mathbb{R}$.

We assume that the curve is equipped with an orthonormal frame and we describe the location of the ruling vectors with respect to this frame. To ensure that the curve's frame is continuous, we define the curve $\mathbf{X}(t)$ through three functions: $K(t) : T \to \mathbb{R}$, $\tau(t) : T \to \mathbb{R}$, and $s(t) : T \to \mathbb{R}$ which define $\mathbf{X}(t)$ up to Euclidean motion through the Frenet-Serret formulas, that is, $\mathbf{X}'(t) = s'(t)\mathbf{T}(t)$, where

$$\begin{pmatrix} \mathbf{T}'(t) \\ \mathbf{N}'(t) \\ \mathbf{B}'(t) \end{pmatrix} = s'(t) \begin{pmatrix} 0 & K(t) & 0 \\ -K(t) & 0 & \tau(t) \\ 0 & -\tau(t) & 0 \end{pmatrix} \begin{pmatrix} \mathbf{T}(t) \\ \mathbf{N}(t) \\ \mathbf{B}(t) \end{pmatrix}. \tag{2}$$

Here we require that the $K(t)$, $\tau(t)$, and $s'(t)$ are continuous, and $s'(t) > 0$.

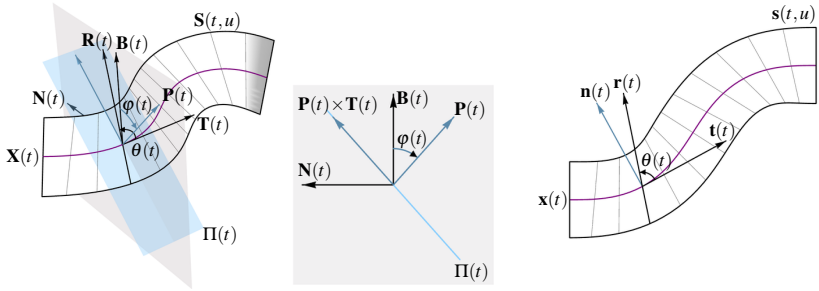

Figure 2: *Illustration of the notation of a developable patch and its development.*

Note that as we allow $K(t)$ to take negative values, the described frame is not a Frenet-frame. Moreover, functions with isolated parameters or intervals where $K(t) = 0$ or $\tau(t) = 0$ still yield a continuous frame $(\mathbf{T}(t), \mathbf{N}(t), \mathbf{B}(t))$. Nevertheless, at parameter values where the Frenet-frame is defined, the computed frame coincides with the Frenet-frame, differing only by sign. Moreover, $K(t)$ corresponds to the curvature of the directrix up to sign, while $\tau(t)$ is the torsion of the directrix when defined.

To determine the ruling directions with respect to the frame $(\mathbf{T}(t), \mathbf{N}(t), \mathbf{B}(t))$, we introduce two additional angular functions: the *inclination angle* $\varphi(t) : T \to \mathbb{R}$ and the *ruling angle* $\theta(t) : T \to [0, \pi)$; see Figure 2.

The inclination angle $\varphi(t)$ encodes the angle between a one-parameter family of planes $\Pi(t)$, which contain the curve's tangent vectors $\mathbf{T}(t)$. Those planes will correspond to the tangent planes if the ruled surface is developable. We express the normal vector $\mathbf{P}(t)$ of $\Pi(t)$ as

$$\mathbf{P}(t) = \cos\varphi(t)\ \mathbf{B}(t) + \sin\varphi(t)\ \mathbf{N}(t), \tag{3}$$

resulting in $\varphi(t)$ being the signed angle between $\mathbf{P}(t)$ and $\mathbf{B}(t)$.

Within the plane $\Pi(t)$, we locate the ruling direction using the ruling angle as

$$\begin{aligned}\mathbf{R}(t) &= \cos\theta(t)\ \mathbf{T}(t) + \sin\theta(t)\,(\mathbf{P}(t) \times \mathbf{T}(t)) \\ &= \cos\theta(t)\ \mathbf{T}(t) + \sin\theta(t)\,(\cos\varphi(t)\ \mathbf{N}(t) - \sin\varphi(t)\ \mathbf{B}(t))\,.\end{aligned} \tag{4}$$

In the following computations, we require both $\theta(t)$ and $\varphi(t)$ to be C^1. Additionally, we will assume that $\theta(t) : T \to (0, \pi)$, excluding cases where $\mathbf{R}(t)$ is aligned with the tangent $\mathbf{T}(t)$ of $\mathbf{X}(t)$.

2.1.2 Developability Condition and Development

It is known that the ruled surface in Equation (1) is developable if for all rulings, the tangent planes along points on a ruling are the same [Pottmann and Wallner 10, Mundilova 23]. This condition can be expressed as the $\det(\mathbf{X}'(t), \mathbf{R}(t), \mathbf{R}'(t)) = 0$. Using the Frenet-Serret equations in Equation (2) and Equation (4), this condition

simplifies to

$$\frac{\varphi'(t)}{s'(t)} = \tau(t) + K(t)\sin\varphi(t)\cot\theta(t); \tag{5}$$

see [Mundilova 23] for more details.

Given a *developable surface* $\mathbf{S}(t,u)$, that is, a ruled surfaces satisfying the above equation, we will parametrize its flattened configuration, the *development*, by $\mathbf{s}(t,u) = \mathbf{x}(t) + u\mathbf{r}(t)$, where $\mathbf{x}(t) : T \to \mathbb{R}^2$ represents the 2D counterpart of the directrix $\mathbf{X}(t)$, and $\mathbf{r}(t) : T \to S^1$ the unit-length 2D ruling direction; see Figure 2.

To obtain the developed directrix $\mathbf{x}(t)$, we consider the *geodesic curvature* of $\mathbf{X}(t)$ as a curve on $\mathbf{S}(t,u)$, that is, the curvature of the projection of $\mathbf{X}(t)$ on $\Pi(t)$ at parameter t,

$$k(t) = K(t)\cos\varphi(t). \tag{6}$$

We obtain $\mathbf{x}(t)$ by determining the 2D curve with signed curvature $k(t)$ and parametrization speed $s'(t)$. This amounts in solving the system of differential equations $\mathbf{x}'(t) = s'(t)\mathbf{t}(t)$, where

$$\begin{pmatrix}\mathbf{t}'(t)\\ \mathbf{n}'(t)\end{pmatrix} = s'(t)\begin{pmatrix}0 & k(t)\\ -k(t) & 0\end{pmatrix}\begin{pmatrix}\mathbf{t}(t)\\ \mathbf{n}(t)\end{pmatrix}. \tag{7}$$

Note that a solution $\mathbf{n}(t)$ points to the "left" side of $\mathbf{t}(t)$, and thus $k(t)$ corresponds to the signed curvature in the developed state in [Demaine et al. 18]. As isometry preserves angles on surfaces, particularly the oriented angle between $\mathbf{T}(t)$ and $\mathbf{R}(t)$ or $\mathbf{P}(t)\times\mathbf{T}(t)$, the developed (left-side) ruling directions read

$$\mathbf{r}(t) = \cos\theta(t)\ \mathbf{t}(t) + \sin\theta(t)\ \mathbf{n}(t).$$

2.1.3 Ruling Curvature

In subsequent sections, we will consider bend configurations $\mathbf{S}(t,u)$ of a planar developable patch $\mathbf{s}(t,u)$ with specified rulings. To show that two such configurations are identical, we calculate the curvature that indicates the surface's bend perpendicular to the rulings, following the methodology of [Demaine et al. 15b, Demaine et al. 18]. This *ruling curvature* is the normal curvature at a given point on an arc-length parametrized curve perpendicular to the rulings at parameter t, expressed as:

$$V(t) = s'(t)k(t)\tan\varphi(t)\frac{1}{\sin\theta(t)}. \tag{8}$$

Up to Euclidean motion, a 3D configuration of a planar developable patch with specified rulings is determined by its ruling curvature.

2.2 Folding a Single Curved Crease

Folding a flat piece of material along a single curved crease, denoted by $\mathbf{x}(t)$, offers considerable flexibility. However, specifying the rulings for the two surface patches incident to the crease narrows the folding motion down to a one-parameter family of 3D configurations corresponding to this development. We will now revise the computation of these configurations.

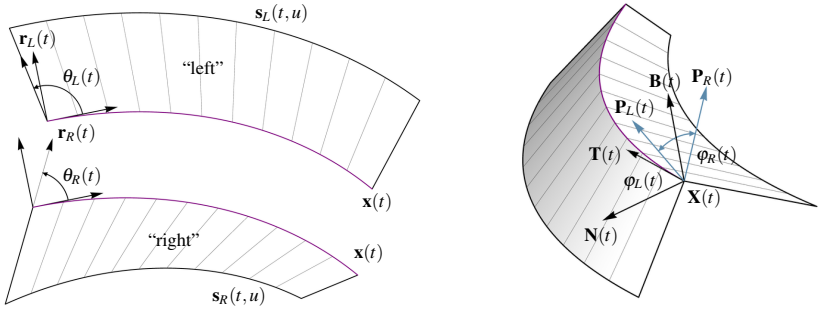

Figure 3: *Illustration of the notation introduced in Section 2.*

2.2.1 Notation

A curved crease, denoted as $\mathbf{x}(t)$, locally divides the sheet into two sides, a "left" and "right" side with respect to the orthonormal frame of the common curve,

$$\mathbf{s}_L(t,u) = \mathbf{x}(t) + u\mathbf{r}_L(t) \qquad \text{and} \qquad \mathbf{s}_R(t,u) = \mathbf{x}(t) - u\mathbf{r}_R(t),$$

where $\mathbf{r}_j(t) = \cos\theta_j(t)\ \mathbf{t}(t) + \sin\theta_j(t)\ \mathbf{n}(t)$ for $j \in \{L,R\}$ is the (left-side) ruling direction and $(\mathbf{t}(t),\mathbf{n}(t))$ is the local orthonormal frame; see Figure 3. Let $k(t)$ and $s(t)$ denote the curvature and arc-length of the crease curve $\mathbf{x}(t)$.

2.2.2 Computation

To compute the 3D configuration, that is,

$$\mathbf{S}_L(t,u) = \mathbf{X}(t) + u\mathbf{R}_L(t) \qquad \text{and} \qquad \mathbf{S}_R(t,u) = \mathbf{X}(t) - u\mathbf{R}_R(t),$$

we need to determine the curvature $K(t)$ and torsion $\tau(t)$ of the 3D crease and the inclination angles $\varphi_L(t)$ and $\varphi_R(t)$ of the adjacent surfaces.

Since Equation (6) needs to be satisfied by both inclination angles, it follows that $\cos\varphi_L(t) = \cos\varphi_R(t)$. The interesting "folded" case occurs when $\varphi(t) = \varphi_L(t) = -\varphi_R(t)$ [Fuchs and Tabachnikov 99]. In this case, we consider the developability condition (Equation (5)) for both incident surfaces and Equation (6). Solving for $\varphi'(t)$, $\tau(t)$, and $K(t)$ results in

$$\varphi'(t) = \frac{1}{2}s'(t)k(t)\left(\cot\theta_R(t) + \cot\theta_L(t)\right)\tan\varphi(t), \tag{9}$$

$$\tau(t) = \frac{1}{2}s'(t)k(t)\left(\cot\theta_R(t) - \cot\theta_L(t)\right)\tan\varphi(t), \tag{10}$$

$$K(t) = \frac{k(t)}{\cos\varphi(t)}. \tag{11}$$

The function $2\varphi(t)$ quantifies the deviation from a configuration in which the tangent planes are aligned, indicating a state where the paper is locally uncreased.

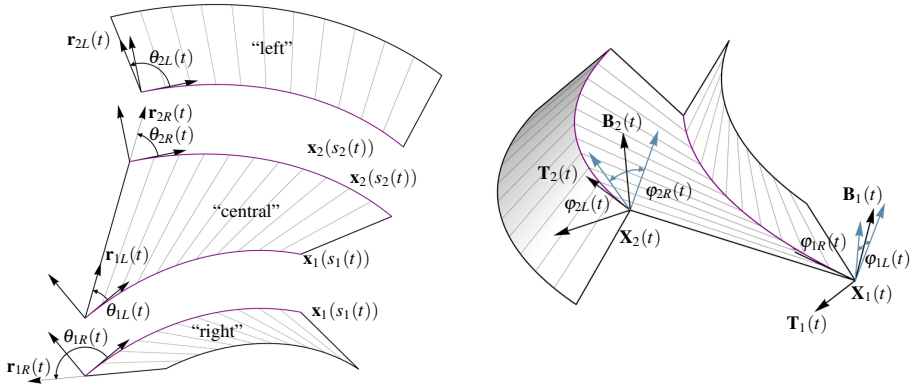

Figure 4: *Illustration of the notation introduced in Section 3.*

Consequently, $\varphi(t)$ represents *half of the fold angle*. Additionally, it is important to note that $\varphi(t)$ is determined by the differential equation in Equation (9) up to the initial value[1]. Upon successful computation of the inclination angle $\varphi(t)$, the curvature and torsion of $\mathbf{X}(t)$ follow from Equation (10) and Equation (11).

The 3D configuration is then obtained by solving the Frenet-Serret equations in Equation (2) and constructing the corresponding 3D ruling directions $\mathbf{R}_L(t)$ and $\mathbf{R}_R(t)$ (Equation (4)) for appropriate inclination and ruling angles[2].

3 Computation of Rulings Between Two Known Patches

We are now interested in computing the shape that results from folding along two crease curves. Similar to the case with a single crease, the shape would exhibit significant flexibility if no rulings were prescribed. However, prescribing the rulings for all three patches could result in an overconstrained system. This issue arises because each pair of adjacent patches functions as a one-degree-of-freedom mechanism, which may not lead to a congruent configuration of the shared surface.

To address this, it becomes necessary to introduce some flexibility into the 2D pattern. Below, we present one approach; for other approaches see [Mundilova 23]. Specifically, we prescribe the rulings of the outer surfaces while allowing the rulings of the central patch to remain flexible.

[1] In fact, the inclination can be obtained as

$$\varphi(t) = \arcsin\left(c_0 e^{\int_0^t f(\bar{t})d\bar{t}}\right) \qquad \text{where} \qquad f(t) = \frac{1}{2}s'(t)k(t)\left(\cot\theta_L(t) + \cot\theta_R(t)\right)$$

and $c_0 = \sin\varphi(0)$ is an appropriate initial value. For $\varphi(t)$ to be real-valued for all $t \in T$, we require

$$|c_0| \leq c_{\max} = \min_{t\in T} e^{-\int_0^t f(\bar{t})d\bar{t}}.$$

[2] Since typically $c_{\max} > 0$, there generally exists a one-parameter family of suitable fold angles in the vicinity of the flat state.

3.1 Notation

In the following, let $\mathbf{x}_1(s)$ and $\mathbf{x}_2(s)$ be two arc-length parametrized creases, such that $\mathbf{x}_2(s)$ is to the "left" of $\mathbf{x}_1(s)$. Furthermore, let the rulings of the right surface $\mathbf{s}_{1R}(s,u)$ of $\mathbf{x}_1(s)$ and left surface $\mathbf{s}_{2L}(s,u)$ of $\mathbf{x}_2(s)$ be specified, meaning that $\mathbf{r}_{1L}(s)$ and $\mathbf{r}_{2R}(s)$ are given; see Figure 4. Let $k_i(s)$ be the curvatures of the arc-length parametrized curves $\mathbf{x}_i(s)$.

To encode flexible rulings in the central patch, we follow the approach by [Demaine et al. 18]. We introduce a parameter t and two functions $s_1(t)$ and $s_2(t)$ such that the rulings of the central patch, which is parametrized by both $\mathbf{s}_{1L}(t,u)$ and $\mathbf{s}_{2R}(t,u)$, are spanned by $\mathbf{x}_1(s_1(t))$ and $\mathbf{x}_2(s_2(t))$, that is,

$$\mathbf{r}_{1L}(t) = \mathbf{r}_{2R}(t) = \frac{\mathbf{x}_2(s_2(t)) - \mathbf{x}_1(s_1(t))}{|\mathbf{x}_2(s_2(t)) - \mathbf{x}_1(s_1(t))|}. \tag{12}$$

It follows that the ruling angles of the central surface relative to either curve can be determined as

$$\theta_{1L}(t) = \arctan\left(\mathbf{t}_{1L}(s_1(t)) \cdot \mathbf{r}_{1L}(t), \mathbf{n}_{1L}(s_1(t)) \cdot \mathbf{r}_{1L}(t)\right), \tag{13}$$

$$\theta_{2R}(t) = \arctan\left(\mathbf{t}_{2R}(s_2(t)) \cdot \mathbf{r}_{2R}(t), \mathbf{n}_{2R}(s_2(t)) \cdot \mathbf{r}_{2R}(t)\right). \tag{14}$$

Here, $\mathbf{t}_i(s)$ represents the unit tangent, while $\mathbf{n}_i(s)$ stands for the (left-side) normal of $\mathbf{x}_1(s)$ and $\mathbf{x}_2(s)$, respectively. Moreover, let $\theta_{1R}(t)$ and $\theta_{2L}(t)$ be the ruling angles corresponding to $\mathbf{r}_{1R}(s_1(t))$ and $\mathbf{r}_{2L}(s_2(t))$, respectively.

In conclusion, the development is locally parametrized by the four surfaces

$$\mathbf{s}_{ij}(t,u) = \mathbf{x}_i(t) + u\sigma_j \mathbf{r}_i(t),$$

where $i \in \{1,2\}$, $j \in \{L,R\}$, $\sigma_L = +1$, and $\sigma_R = -1$.

3.2 Computation

In the following, we aim to describe the geometry of the two fold curves $\mathbf{X}_1(t)$ and $\mathbf{X}_2(t)$ and the incident patches. Consequently, it is necessary to establish a relationship between $s_1(t)$ and $s_2(t)$, typically by assuming $s_1(t) = t$ and then determining $s_2(t)$. We must also calculate the curvatures $K_1(t)$ and $K_2(t)$, the torsions $\tau_1(t)$ and $\tau_2(t)$, and the inclination angles $\varphi_{1L}(t)$, $\varphi_{1R}(t)$, $\varphi_{2L}(t)$, and $\varphi_{2R}(t)$.

We begin our computation by considering Equation (6). This equation must be satisfied for the patches incident to both curves $\mathbf{X}_1(t)$ and $\mathbf{X}_2(t)$. As in the previous analysis, the interesting case occurs when $\varphi_i(t) = \varphi_{iL}(t) = -\varphi_{iR}(t)$, linking the 2D and 3D curvatures through

$$k_i(s_i(t)) = K_i(t)\cos\varphi_i(t). \tag{15}$$

Additionally, similarly to before, we require that the 3D configurations of the four surfaces, $\mathbf{s}_{1L}(t,u)$, $\mathbf{s}_{1R}(t,u)$, $\mathbf{s}_{2L}(t,u)$, and $\mathbf{s}_{2R}(t,u)$, are developable. Consequently, for $i \in \{1,2\}$ and $j \in \{L,R\}$, Equation (5) simplifies to

$$\frac{\varphi_i'(t)}{s_i'(t)} = \sigma_{ij}\tau_i(t) + K_i(t)\sin\varphi_i(t)\cot\theta_{ij}(t), \tag{16}$$

where $\sigma_{iL} = +1$ and $\sigma_{iR} = -1$.

Finally, we want to ensure that the two surfaces $\mathbf{S}_{1L}(t)$ and $\mathbf{S}_{2R}(t)$ belong to the same surface. Consequently, we consider the ruling curvature of the common patch with respect to the directrices $\mathbf{X}_1(t)$ and $\mathbf{X}_2(t)$, with the goal to ensure that their principal curvatures are the same, that is,

$$s_1'(t)K_1(t)\sin\varphi_1(t)\frac{1}{\sin\theta_{1L}(t)} = -s_2'(t)K_2(t)\sin\varphi_2(t)\frac{1}{\sin\theta_{2R}(t)}. \tag{17}$$

Solving the system of seven equations in Equation (15), Equation (16), and Equation (17) for the seven unknowns, $s_2'(t)$, $\varphi_1'(t)$, $\varphi_2'(t)$, $K_1(t)$, $K_2(t)$, $\tau_1(t)$, and $\tau_2(t)$, yields

$$s_2'(t) = -s_1'(t)\frac{k_1(s_1(t))}{k_2(s_2(t))}\frac{\sin\theta_{2R}(t)}{\sin\theta_{1L}(t)}\frac{\tan\varphi_1(t)}{\tan\varphi_2(t)}, \tag{18}$$

$$\varphi_1'(t) = \frac{1}{2}s_1'(t)k_1(s_1(t))\left(\cot\theta_{1L}(t) + \cot\theta_{1R}(t)\right)\tan\varphi_1(t), \tag{19}$$

$$\varphi_2'(t) = -\frac{1}{2}s_1'(t)k_1(s_1(t))\frac{\sin\left(\theta_{2L}(t)+\theta_{2R}(t)\right)}{\sin\theta_{1L}(t)\sin\theta_{2L}(t)}\tan\varphi_1(t), \tag{20}$$

$$K_i(t) = \frac{k_i(s_i(t))}{\cos\varphi_i(t)}, \tag{21}$$

$$\tau_i(t) = -\frac{1}{2}\left(\cot\theta_{iL}(t) - \cot\theta_{iR}(t)\right)k_i(s_i(t))\tan\varphi_i(t). \tag{22}$$

Note that the first three equations form a system of differential equations for the three unknown functions $s_2(t)$, $\varphi_1(t)$, and $\varphi_2(t)$. With appropriate initial values, the successful computation of these functions specifies the remaining quantities, the curvatures and torsions, through the algebraic equations in Equation (21) and Equation (22). It is important to note that the unknown function $s_2(t)$ serves as a parameter in the curvature of the second developed crease curve. When solving the above differential equations using modern mathematical software, having explicit knowledge of the second curve's developed curvature in terms of its arc-length is beneficial or even necessary.

Finally, the Frenet-Serret equations, as described in Equation (2), can be used to construct the 3D configurations. Here, it is crucial to ensure that the initial values of the differential equations, the initial orthonormal frames, are correctly positioned. Detailed explanations are provided in [Mundilova 23].

4 Analysis of Huffman's Hexagonal Column

David Huffman's Hexagonal Column, depicted in Figure 1 (right), exhibits six-fold rotational symmetry and its crease pattern contains circular, parabolic, and straight creases, as shown in Figure 1 (left). The rotational symmetry suggests that the region between two adjacent parabolic arches is cylindrically ruled. Additionally, the section that connects the intersection of two neighboring parabolas with the

circular arc must be, at the very least, locally conically ruled; see Figure 1 (right). However, the rulings of the central strip are not obvious. In this section, we apply the theory from Section 3 to identify rulings that are (locally) compatible and result in a (numerically) closed shape.

Due to the symmetry of the pattern, we initially restrict our folding analysis only to a part the the crease pattern, which we refer to as *module*, consisting of a parabolic and a circular arc that share the same center and focal point, respectively; see Figure 5a. Specifically, we set the common center to coincide with the origin, choose the circle to have a radius of one, and let the parabola to be symmetric with respect to the x-axis and to pass through the point $(2,0)$.

This section starts by identifying three essential constraints on the folded modules necessary for arranging them into a closed hexagonal shape. Following this, we detail the parametrization of a module's development, setting the groundwork for employing the computational methods discussed in Section 3. We then consider two strategies to determine a single module's folded state. The first strategy, which offers only two degrees of freedom, was experimentally found insufficient to meet the specified three constraints. The second strategy introduces an additional parameter, enabling the computation of a folded state that satisfies all three constraints. This section concludes with a discussion of the numerical results and explores possible variations of the shape.

4.1 Composition of Modules

Upon successfully computing a folded configuration of a module, our goal is to arrange multiple modules to form the complete hexagonal shape. However, this is not feasible for all folded modules, as they must satisfy certain constraints related to their boundary.

To describe the constraints necessary for a folded module's configuration to achieve a closed shape, we identify the following key points in the development[3],

$$\mathbf{o} = (0,0), \quad \mathbf{a} = (2,0), \quad \mathbf{a}' = (0,4), \quad \mathbf{b} = (1,0), \quad \mathbf{b}' = (0,1), \quad \mathbf{c} = (2,4),$$

and denote their location on a folded configuration by upper-case letters, $\mathbf{O}$, $\mathbf{A}$, $\mathbf{A}'$, $\mathbf{B}$, $\mathbf{B}'$, and $\mathbf{C}$; see Figure 5a.

The possibility of arranging the modules into a hexagonal shape can be simplified to finding a configuration where two modules positioned "vertically" align between two planes at a suitable opening angle; see Figure 5b. Specifically, let T be the transformation that aligns the ordered triples of points $(\mathbf{A},\mathbf{B},\mathbf{O})$ with $(\mathbf{O},\mathbf{B},\mathbf{A})$. When applying T to a copy of a folded module, we obtain two "vertically" aligned modules. Let furthermore Π represent the base plane of the cylinder, that is, a plane perpendicular to $\mathbf{R} := \mathbf{A}' - \mathbf{C}$ passing through $\mathbf{C}$.

The requirement that two vertically aligned modules can be wedged between two planes, Π and $T(\Pi)$, can be ensured by the following two constraints:

[3]These points reflect the dimensions in David Huffman's original sketches shown in Figure 4.4.46 and Figure 4.4.47 in [Koschitz 14].

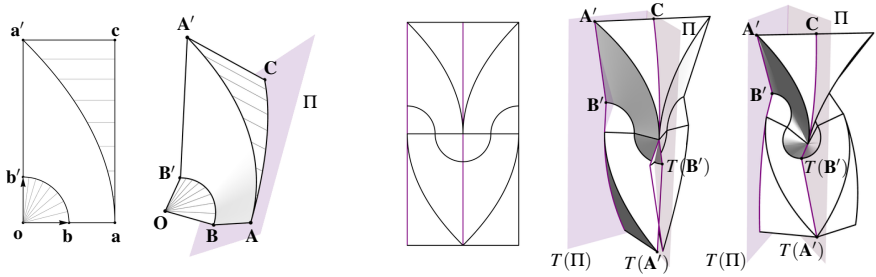

(a) *One module and a illustration of a folded state.*

(b) *Composition of four modules: development, not aligned and aligned configuration.*

Figure 5: *Illustration of a module and two compositions of four copies.*

- *Constraint 1:* $T(\mathbf{A}') \in \Pi$. We measure the corresponding error e_1 by computing the absolute distance between $T(\mathbf{A}')$ and Π.
- *Constraint 2:* $T(\mathbf{B}') \in \Pi$. Again, we measure the corresponding error e_2 by computing the absolute distance between $T(\mathbf{B}')$ and Π.

In case of a hexagonal base, we additionally require that the planes have appropriate opening angle, consequently:

- *Constraint 3:* The angle between $\mathbf{R}$ and $T(\mathbf{R})$ should be $\frac{5\pi}{6}$. We define the corresponding error as $e_3 = \left|\mathbf{R} \cdot T(\mathbf{R}) - \cos\frac{5\pi}{6}\right|$.

It follows that a folded module satisfying the three constraints allows a composition into a closed hexagonal shape.

4.2 Parametrization of the Development of a Module

To apply the method discussed in Section 3, we denote the arc-length parametrization of the parabolic arc by $\mathbf{x}_1(s)$, starting with $s_{\min} = 0$ at $\mathbf{a}$ and ending[4] with $s_{\max} \approx 4.59117$ at $\mathbf{a}'$, and numerically compute its curvature $k_1(s)$. Let $\mathbf{x}_2(s)$ denote the arc-length parametrization of the circle,

$$\mathbf{x}_2(s) = (\cos s, \sin s)\,,$$

resulting in the constant curvature $k_2(t) = 1$. To ensure that the curvature corresponding to the unknown arc-length parameter can be explicitly stated, we set

[4] For $t \in \left[0, \frac{\pi}{2}\right]$, the parabolic arc can be parametrized by

$$\mathbf{p}(t) = \frac{4}{1+\cos t}\,(\cos t, \sin t)\,.$$

Its arc-length can be computed as

$$s_1(t) = \int_0^t \left|\mathbf{p}'(u)\right| du = 2\int_0^t \left(\cos\frac{u}{2}\right)^{-3} du = 2\left(\operatorname{arctanh}\left(\sin\frac{t}{2}\right) + \frac{\tan\frac{t}{2}}{\cos\frac{t}{2}}\right).$$

Consequently, $s_{\max} = s_1\left(\frac{\pi}{2}\right) \approx 4.59117$.

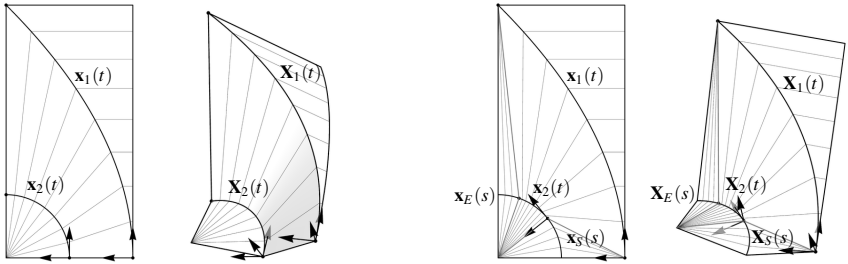

(a) *No singularities.* **(b)** *With singularities.*

Figure 6: *Development and folded configurations of the considered modules, illustrating central surfaces with either no or two singularities.*

$s_1(t) = t$ with the goal of determining $s_2(t)$. Consequently, we let the parameter t have the same range as the arc-length parameter of $\mathbf{x}_1(s)$, hence $t \in [0, t_{\max}]$ where $t_{\max} \approx 4.59117$.

Following our assumptions about the rulings of the folded shape, we set the ruling directions of the left and right patches to be conical and cylindrical, respectively. Consequently,

$$\mathbf{r}_{1R}(t) = (-1, 0) \qquad \text{and} \qquad \mathbf{r}_{2L}(t) = -\frac{\mathbf{x}_2(s_2(t))}{|\mathbf{x}_2(s_2(t))|}.$$

The corresponding ruling angles read

$$\theta_{1R}(t) = \arctan\left(\mathbf{r}_{1R}(t) \cdot \mathbf{t}_1(t), \mathbf{r}_{1R}(t) \cdot \mathbf{n}_1(t)\right)$$
$$\theta_{2L}(t) = \arctan\left(\mathbf{r}_{2L}(t) \cdot \mathbf{t}_2(s_2(t)), \mathbf{r}_{2L}(t) \cdot \mathbf{n}_2(s_2(t))\right)$$

where $\mathbf{t}_i(s)$ and $\mathbf{n}_i(s)$ denote the tangent and normal vectors of $\mathbf{x}_i(s)$. Finally, we use Equation (12) to define the ruling direction $\mathbf{r}_{1L}(t) = \mathbf{r}_{2R}(t)$ of the central patch, and use Equation (13) and Equation (14) to define their corresponding ruling angles $\theta_{1L}(t)$ and $\theta_{2R}(t)$.

This concludes our preparations regarding the parametrization of the development in Section 3.1, and sets the stage for the computations described in Section 3.2.

4.3 Computation of a Folded Module

We now use the equations in Section 3.2 to compute the folded states of a single module. Through experimental observation, we find that folded states without singular points do not possess sufficient flexibility to meet the necessary constraints. Consequently, we consider variations with singularities to (numerically) satisfy the three required constraints.

4.3.1 Folded Modules without Singularities

In our first approach, we attempt to populate the central surface with rulings without introducing additional singularities, as illustrated in Figure 6a. Consequently, when solving the system of differential equations presented in Equations (18)-(20) to compute the inclination angles and the unknown parametrization speed, we initialize $s_2(0) = 0$. Additionally, we select appropriate initial values for $\varphi_1(t)$ and $\varphi_2(t)$.

The choice of initial values for the inclination angles impacts the value of $s_2(t_{\max})$. To ensure complete coverage of the central patch, the solution $s_2(t)$ must satisfy $s_2(t_{\max}) = \frac{\pi}{2}$. In addition to the three constraints described in Section 4.1, this introduces a fourth constraint. However, we have only two parameters to adjust, namely the two initial values of the inclination angles. Experimentally, we were unable to find a combination of the two initial values that would result in a folded module that satisfies all four constraints.

4.3.2 Folded Modules with Singularities

To eliminate the fourth constraint and introduce a new parameter, we adjusted our approach by allowing variations in the initial value of $s_2(0)$, within reasonable bounds ($0 < s_2(0) < \frac{\pi}{2}$). This adjustment, however, results in the central surface not being fully covered. To compensate for this, we fill the gaps at the beginning and end with conical surfaces connected along circular creases.

Next, we will briefly demonstrate how to attach these two conical patches at the beginning and end, and discuss the corresponding computation.

Modified parametrization of the development. We divide the circular arc into three parts. In the following, we use subscripts "S" and "E" to indicate whether the newly introduced circular creases belong to the "start", that is, the circular segment $\mathbf{x}_S(s) = \mathbf{x}_2(s)$ where $s \in [0, s_2(0)]$, or "end", that is, the circular segment $\mathbf{x}_E(s) = \mathbf{x}_2(s)$ where $s \in [s_2(t_{\max}), \frac{\pi}{2}]$.

We define the ruling directions of the left patches to be

$$\mathbf{r}_{S,L}(s) = \mathbf{r}_{E,L}(s) = -\frac{\mathbf{x}_2(s)}{|\mathbf{x}_2(s)|}.$$

In addition, we define the ruling directions of the right patches as

$$\mathbf{r}_{S,R}(s) = \frac{\mathbf{x}_2(s) - \mathbf{x}_1(0)}{|\mathbf{x}_2(s) - \mathbf{x}_1(0)|} \qquad \text{and} \qquad \mathbf{r}_{E,R}(s) = \frac{\mathbf{x}_2(s) - \mathbf{x}_1(t_{\max})}{|\mathbf{x}_2(s) - \mathbf{x}_1(t_{\max})|}.$$

The corresponding ruling angles $\theta_{S,R}(t)$, $\theta_{S,L}(t)$, $\theta_{E,R}(t)$ and $\theta_{E,L}(t)$ follow similar to Equation (13) and Equation (14).

Modified computation of the 3D configuration. The modified computation proceeds as follows: First, we calculate the parametrization speed and inclination angles of the central patch using the method outlined in Section 3.2. This method provides information on the lengths of the circular segments, $\mathbf{x}_S(t)$ and $\mathbf{x}_E(t)$.

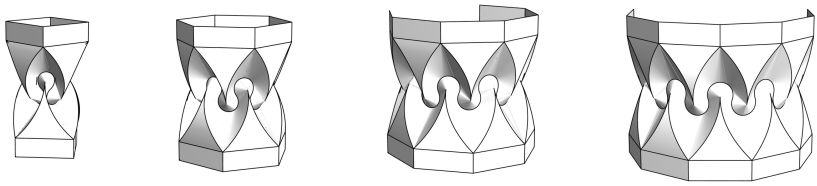

Figure 7: *Hexagonal Column variations for angles α_n where $n \in (2,3,4,5)$.*

For both sides, we then compute $\varphi_S(t)$ and $\varphi_E(t)$ as described in Section 2.2.2. To achieve tangent-continuous transitions, we require continuous inclination angles. Consequently, we set the initial values of the inclination angles with the corresponding start and end values of $\varphi_2(t)$, that is, we set $\varphi_S(s_2(0)) = \varphi_2(0)$ and $\varphi_E(s_2(t_{\max})) = \varphi_2(t_{\max})$.

Finally, to ensure tangent-continuous transitions when computing the 3D configuration of the crease curve , we begin the integration of the Frenet-Serret equations at the frames located at the endpoints of $\mathbf{X}_2(t)$. After successfully computing the crease, we then proceed to construct the left and right ruling directions.

In conclusion, the modified approach provides us with three parameters to adjust that fully specify a folded configuration of the module: the initial values of the functions $s_2(t)$, $\varphi_1(t)$, and $\varphi_2(t)$. These adjustments allow us to address the three constraints outlined in Section 4.1.

4.4 Numerical Results and Discussion

Using numerical minimization in Mathematica (with manual help to find a good initial guess), we obtain the following initial values and corresponding error measurements,

$$\begin{pmatrix} s_2(0) \\ \varphi_1(0) \\ \varphi_2(0) \end{pmatrix} = \begin{pmatrix} 0.6015913936768009 \\ -0.7753374025984491 \\ 0.6754673354175101 \end{pmatrix} \quad \text{and} \quad \begin{pmatrix} e_1 \\ e_2 \\ e_3 \end{pmatrix} = \begin{pmatrix} 1.4 \cdot 10^{-9} \\ 1.02 \cdot 10^{-10} \\ 6.22 \cdot 10^{-15} \end{pmatrix},$$

respectively.

Consequently, the folded module, corresponding to these initial values, allows for an arrangement into a numerically closed shape, as shown in Figure 1. To better align with David Huffman's design, we added planar faces at the top and bottom of the shape.

Note, however, that although our results are derived from computations using smooth functions, the underlying mathematical program employs three operations that may involve discretization sequentially – specifically, the computation of $k_1(s)$ and two numerical integration steps – thereby inherently introducing numerical errors into the computations. Consequently, while our analysis does not permit a rigorous statement regarding the existence of the Hexagonal Column, it nevertheless provides some indications of its potential existence.

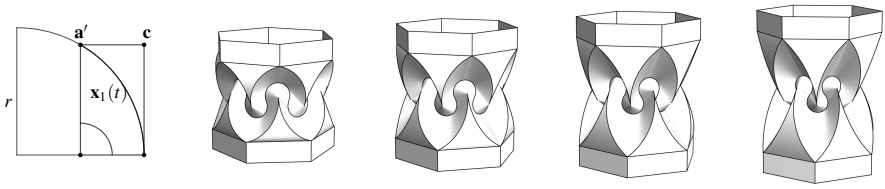

Figure 8: *Hexagonal Column with parabolic arcs substituted by circular arcs of radii* $r \in (3,4,5,6)$.

4.5 Variations

Finally, we explore two possible ways to generate variations of the Hexagonal Column.

Other regular polygonal bases. David Huffman's work also features columns with quadrangular bases, as opposed to hexagonal ones, as outlined by [Koschitz 14]. By generalizing the third constraint in Section 4.1 to an angle $\alpha_n = \frac{(2n-1)\pi}{2n}$ with $n \geq 2$, upon successful computation of $s_2(0)$, $\varphi_1(0)$, and $\varphi_2(0)$, we can arrange folded modules into columns with a $2n$-gonal base; see Figure 7. Experimental observations indicate that the value of $s_2(0)$ changes across different target opening angles, suggesting the absence of a rigid-ruling folding motion.

Circular curves. Another variation of the pattern includes replacing the parabolic crease with a circular arc of radius r; see Figure 8 (left). In this case we have $\mathbf{a}' = \left(0, \sqrt{3}r/2\right)$ and $\mathbf{c} = \left(2, \sqrt{3}r/2\right)$. We observed very similar behavior in the rulings of the central patch, and examples of closed columns with this modification are displayed in Figure 8 (right).

5 Open Problems and Future Work

This analysis was conducted under the assumption that the rulings between a circular arc and the intersection of parabolas are conical. However, this raises the question of whether such an assumption is necessary and whether alternative rulings could result in a closed column. Another avenue for future research involves enhancing the numerical framework to more rigorously establish the (mathematical) existence of the Hexagonal Column.

References

[Alese 22] Leonardo Alese. "Propagation of curved folding: the folded annulus with multiple creases exists." *Beiträge zur Algebra und Geometrie/Contributions to Algebra and Geometry* 63:1 (2022), 19–43.

[Demaine et al. 15a] Erik D. Demaine, Martin Demaine, Duks Koschitz, and Tomohiro Tachi. "A review on curved creases in art, design and mathematics." *Symmetry: Culture and Science* 26:2 (2015), 145–161.

[Demaine et al. 15b] Erik D. Demaine, Martin L. Demaine, David A. Huffman, Duks Koschitz, and Tomohiro Tachi. "Characterization of curved creases and rulings: Design and analysis of lens tessellations." In *Origami*^{6}*: Proceedings of the 6th International Meeting on Origami in Science, Mathematics and Education (OSME 2015)*, pp. 209–230, 2015.

[Demaine et al. 18] Erik D. Demaine, Martin L. Demaine, David A. Huffman, Duks Koschitz, and Tomohiro Tachi. "Conic crease patterns with reflecting rule lines." In *Origami*^{7}*: Proceedings of the 7th International Meeting on Origami in Science, Mathematics and Education (OSME 2018)*, pp. 573–590, 2018.

[Fuchs and Tabachnikov 99] Dmitry Fuchs and Serge Tabachnikov. "More on paperfolding." *The American Mathematical Monthly* 106:1 (1999), 27–35.

[Kergosien et al. 94] Yannick L Kergosien, Hironobu Gotoda, and Tosiyasu L Kunii. "Bending and creasing virtual paper." *IEEE Computer graphics and applications* 14:1 (1994), 40–48.

[Koschitz 14] Duks Koschitz. "Computational design with curved creases: David Huffman's approach to paperfolding." Ph.D. thesis, MIT, 2014.

[Mosely 02] Jeannine Mosely. "The validity of the Orb, an Origami Model." In *Third International Meeting of Origami Science, Mathematics, and Education, AK Peters, Ltd*, pp. 75–82, 2002.

[Mundilova and Wills 18] Klara Mundilova and Tony Wills. "Folding the Vesica Piscis." In *Proceedings of Bridges 2018: Mathematics, Art, Music, Architecture, Education, Culture*, pp. 535–538, 2018.

[Mundilova 23] Klara Mundilova. "Gluing and Creasing Paper along Curves: Computational Methods for Analysis and Design." Ph.D. thesis, Massachusetts Institute of Technology, 2023.

[Pottmann and Wallner 10] Helmut Pottmann and Johannes Wallner. *Computational Line Geometry*. Mathematics and Visualization, Springer Berlin Heidelberg, 2010.

Klara Mundilova
klaramundilova.com, e-mail: klara.mundilova@alum.mit.edu

Erik D. Demaine
Massachusetts Institute of Technology, Cambridge, USA, e-mail: edemaine@mit.edu

Robert J. Lang
Lang Origami, Altadena, USA, e-mail: robert@langorigami.com

Tomohiro Tachi
The University of Tokyo, Tokyo, Japan, e-mail: tachi@idea.c.u-tokyo.ac.jp